Nanoscale

Multifunctional Composite Films with Vertically Aligned ZnO Nanowires by Leaching-enabled Capillary Rise Infiltration

Journal:	*Nanoscale*
Manuscript ID	NR-ART-08-2019-007183.R1
Article Type:	Paper
Date Submitted by the Author:	25-Oct-2019
Complete List of Authors:	Tran, Hong Huy; Grenoble INP Venkatesh, R.; University of Pennsylvania Kim, Youngjin; Grenoble INP Riassetto, David; Grenoble INP Lee, Daeyeon; University of Pennsylvania,

Multifunctional Composite Films with Vertically Aligned ZnO Nanowires by Leaching-enabled Capillary Rise Infiltration

Hong Huy Tran,[a] R. Bharath Venkatesh,[b] Youngjin Kim,[a] Daeyeon Lee*[b] and David Riassetto*[a]

[a] *Univ. Grenoble Alps, CNRS, Grenoble INP [†], LMGP, 38000 Grenoble, France*

[†] *Institute of Engineering Univ. Grenoble Alps*

[b] *Department of Chemical and Biomolecular Engineering,*

University of Pennsylvania, Philadelphia, Pennsylvania 19104, USA

** Corresponding authors: daeyeon@seas.upenn.edu and david.riassetto@grenoble-inp.fr*

ABSTRACT

Nanocomposite films (NCFs) with vertically aligned nanowires (NWs) provide several useful properties owing to their unique morphology. One of the key challenges in producing such an NCF is retaining the vertical alignment of NWs during NCF fabrication. Although current methods such as layer-by-layer assembly and solution-based processes with field-induced alignment of NWs have been successfully demonstrated, these approaches require multiple steps thus are time-consuming, and only suitable for lab-scale production, consequently limiting their widespread applicability. Herein, we describe a new method for fabricating an NCF with vertically aligned ZnO NWs by inducing leaching-enabled capillary rise infiltration (LeCaRI) of uncross-linked and mobile oligomer chains from a poly(dimethylsiloxane) (PDMS) slab into the space between the vertically aligned ZnO NWs. PDMS-infiltrated ZnO NW NCFs have a suite of useful properties including superhydrophobicity, self-cleaning, solvent resistance, and anti-icing properties as well as high transparency and anti-reflection properties. The NCF can easily recover its superhydrophobicity after it has been compromised through repeated plasma treatments or even exposure to intense UV irradiation. Moreover, our approach represents a straightforward, efficient, and potentially scalable strategy to produce multifunctional NCFs with vertically aligned NW arrays which could be easily extended to other types of materials and NW arrangements toward a wide range of properties and applications.

KEYWORDS: *anti-icing, solvent resistance, superhydrophobicity, capillarity, self-cleaning*

INTRODUCTION

Nanocomposite films (NCFs), consisting of inorganic nanomaterials and polymers, represent an important class of functional structures with synergistic properties.[1-11] Unique functionality and emergent properties such as exceptionally high strength and toughness can be achieved by extremely high loadings of nanoparticles (> 50 vol%) as well as the inclusion of anisotropic nanomaterials such as high aspect ratio nanowires (NWs) and their alignment.[3, 4, 7, 12-14] In particular, vertical alignment of high aspect ratio NWs provides a powerful approach to fabricate NCFs with a wide range of useful functionalities owing to its unique morphology.[13-21] Amongst NW materials, zinc oxide (ZnO) NWs, which can be prepared using simple methods such as chemical bath deposition, offer a wide range of useful features such as high strength, photocatalytic, electronic and optical properties.[22-25] NCFs incorporating vertically aligned ZnO NWs, in fact, have demonstrated useful properties owing to their morphology.[13, 17, 25-32] For example, Kim *et al*.[17] designed antireflective layers consisting of vertically aligned ZnO NWs and a polymeric matrix. A polymer precursor was cast onto the surface of the ZnO NWs, followed by a curing step, the cured polymer layer containing ZnO NWs at the outermost surface was then mechanically peeled off from the substrate for applications. More recently, Yeom *et al*.[13] reported the fabrication of a tooth enamel-inspired nanocomposite by filling the interstitial space between vertically oriented ZnO NWs using layer-by-layer

(LbL) assembly. By repeating the growth of ZnO NWs and LbL assembly, light-weight multilayer nanocomposites that exhibit ultra-high stiffness, and vibrational damping were fabricated.

One of the key features that give rise to such useful functionalities to these NCFs is the vertical alignment of the NWs; it is, however, challenging to induce vertical alignment during nanocomposite fabrication. Solution-based processes such as mixing/dispersing NWs are not suitable as the alignment is difficult to achieve without applying an external field such as a magnetic or electric field.[15, 33-35] Given that several methods can directly produce vertically aligned NW arrays on solid surfaces, producing NCFs without detaching the vertically grown NWs from the substrate provides the most straightforward approach to retain the vertical alignment of NWs. As described above, polymer casting followed by curing as well as LbL assembly has been successfully used to produce NCFs based on vertically aligned arrays of ZnO NWs. [13, 16, 36] However, these processes require multiple steps thus are time-consuming, and only suitable for lab-scale production, consequently limiting their widespread applicability.

In this work, we fabricate multifunctional NCFs with vertically aligned ZnO NWs by taking advantage of leaching-enabled capillary rise infiltration (LeCaRI) of uncross-linked and mobile oligomer chains in an elastomer network. The polymer infiltration-based method overcomes the challenges associated with traditional methods of making nanocomposite films. In particular, LeCaRI can be performed while retaining the original configuration of the nanomaterials; thus, by implementing LeCaRI, it is possible to produce NCFs with vertically aligned ZnO NWs in a straightforward manner, making it a potentially scalable manufacturing method. We show that NCFs with vertically aligned ZnO NWs fabricated via LeCaRI have multiple useful properties, including superhydrophobicity, self-cleaning, solvent resistance, anti-icing properties, high transparency, and anti-reflection property. Successful fabrication of multifunctional NCFs with vertically aligned ZnO NWs demonstrates that LeCaRI is a powerful method to produce NCFs with well-controlled arrangements of functional and anisotropic nanomaterials, and can potentially enable scalable manufacturing of multifunctional NCFs with various types of polymers and nanomaterials.

RESULTS AND DISCUSSION

Our method takes advantage of the growth of vertically aligned ZnO NWs on a solid substrate and the infiltration of oligomers from an elastomer network. A recent report has shown that mobile oligomeric species can be induced to undergo infiltration into densely packed nanoparticle films from PDMS network to produce NCFs with extremely high filler fractions (> 50 vol%).[6] Owing to incomplete crosslinking during curing of PDMS, there are a large number of uncross-linked and mobile oligomer chains in the elastomer network.[6, 37-42]. The presence of these uncross-linked and mobile chains in an elastomer network is generally considered as an undesirable feature. However, the ability to induce leaching of these uncross-linked and mobile chains from the elastomer network and inducing their infiltration into interstitial pores between nanomaterials makes it an ideal platform to produce NCFs that retain the original alignment of ZnO NW arrays on the surface. In the present paper, we use PDMS elastomer made from a thermal curing process (at 80 °C for 2h) containing a large number of uncross-linked PDMS oligomer chains for the LeCaRI experiment. The uncross-linked PDMS oligomer chains can leach out of the PDMS elastomer into the surface of and the interstices between ZnO NWs film at room temperature. However, because the thickness of the ZnO NWs film (1.2±0.17 μm) is much greater than that of the SiO_2 nanoparticle films (250 nm) that were used in the previous work, we increase the processing temperature to accelerate the infiltration, resulting in increasing amounts of PDMS oligomer chains transferred from the PDMS elastomer to the ZnO NWs.

The process of fabricating a nanocomposite film (NCF) with vertically aligned ZnO NWs via leaching-enabled capillary rise infiltration (LeCaRI) is schematically presented in Fig. 1. The NCFs are constructed by starting with ZnO-seeded hydrothermal growth of ZnO NWs,[43-45] having a diameter, a length, and a vertical angle of 73±16 nm, 1.2±0.17 µm, and 89±12°, respectively, on glass slides (2.5 cm × 2.5 cm) followed by thermal annealing in the oven at 540 °C for 5 min to remove organic residues and water vapor. ZnO NW arrays are then brought into conformal contact with a slab of PDMS elastomer (2.5 cm × 2.5 cm × 0.25 cm) to induce the transfer of uncross-linked and mobile chains from the elastomer into the crevices of the ZnO NW arrays. To maximize the number of transferred oligomers, the sample with PDMS elastomer atop ZnO NW arrays is placed in an oven maintained at 150 °C. Although the top of the ZnO NW array does not present a very smooth surface, PDMS can be induced to form conformal contact with the ZnO NW array due to its compliance and flexibility. The surface of the ZnO NW array becomes more homogenous after infiltration likely due to the filling of the crevices between NWs by oligomer chains (see SI).

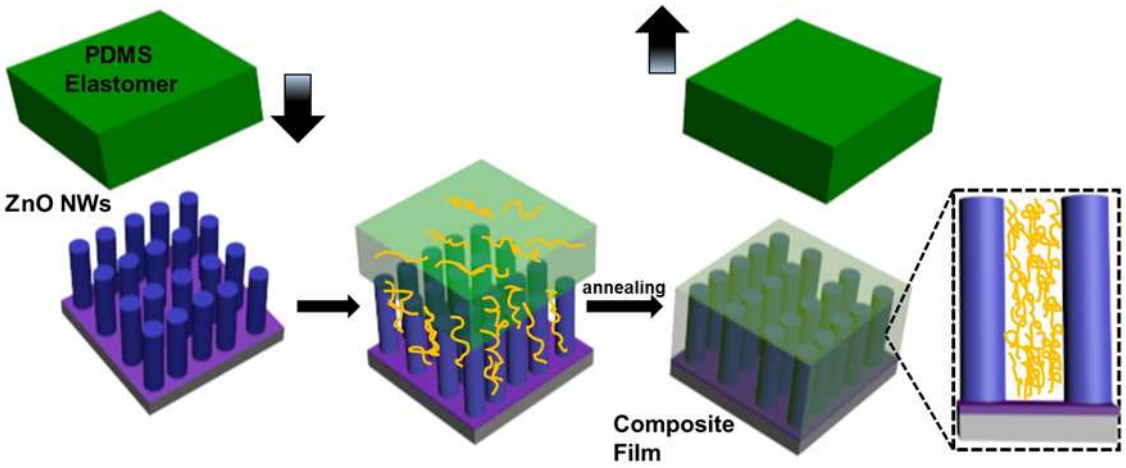

Fig. 1 Schematic illustration showing the LeCaRI process to fabricate nanocomposite films with vertically aligned ZnO NWs. For clarity, schematic illustrations are not drawn to scale.

The morphology of the ZnO NW arrays before and after infiltration for different duration are observed through scanning electron microscopy (SEM) as shown in Fig. 2. The SEM images confirm the presence of PDMS oligomers in the ZnO NW array after LeCaRI. Even after very short infiltration (10 s at room temperature, hereafter referred to as NCF-10s@RT), the interstices and surfaces between NWs have been partially filled by the oligomers, as shown in Fig. 2b, e. For the sample that is subjected to LeCaRI for a long time at a higher temperature (24 h at 150 °C, hereafter referred to as NCF-24h@150 °C), the crevices in the ZnO NW arrays are almost completely filled to form a uniform NCF, as shown in Fig. 2c, f. EDS profiles are provided to confirm the presence of PDMS oligomer chains in the crevices of the ZnO NW arrays, as evidenced by an increase in the amount of silicon in the NCFs after LeCaRI as shown in Fig. 2g-i and in SI, and the amount of PDMS increases with time. The presence of PDMS oligomeric species in the NCF is also confirmed using Raman spectroscopy (see SI for details). Most importantly, ZnO NWs retain their vertical alignment after the LeCaRI process. We also confirm that a similar NCF can be produced by placing an inverted ZnO NW array atop a PDMS slab, illustrating that capillarity is the main driving force for the oligomer infiltration. Despite the filling of the space between ZnO NWs, the top surface of NW array is not fully covered with a visible and smooth layer of PDMS (Fig. 2f) and thus retains the nanoscale surface roughness of the ZnO NW array. As we will show later, such a surface roughness could play an important role in determining the wetting properties of these NCFs.

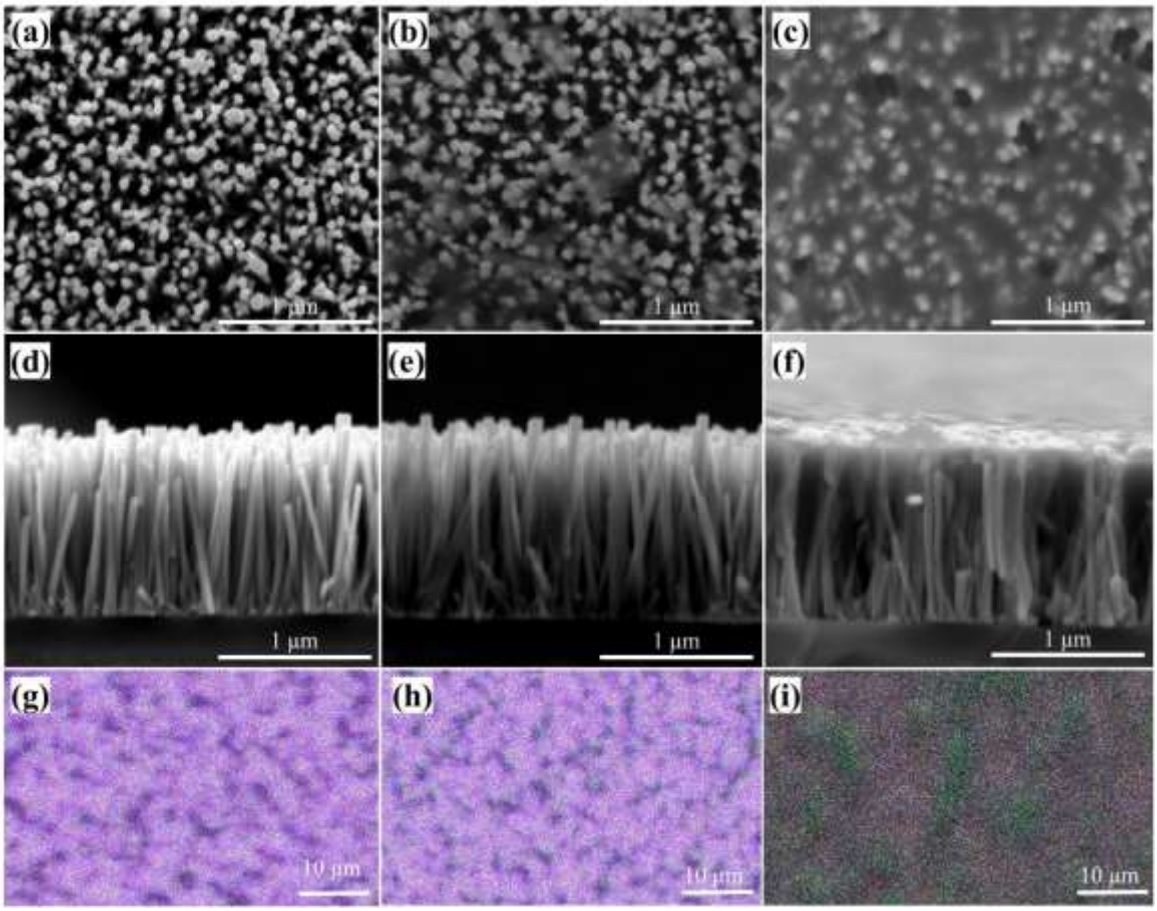

Fig. 2 (a, b, c) Top-view, (d, e, f) cross-section SEM images, and (g, h, i) EDS mapping profiles of ZnO NWs, NCF-10s@RT, and NCF-24h@150 °C, respectively. Green and violet dots represent the presence of Si and Zn, respectively.

One of the disadvantages of using ZnO NW arrays on a solid surface is that they scatter light and thus make it difficult to use them in applications that require high transparency such as coatings on windows and solar cells. With a refractive index of 2.0 for bulk ZnO and a non-continuous morphology, the significant refraction and scattering of incident light at the air−ZnO interface leads to a significant transmittance loss through ZnO NW arrays.[46] Infiltration of PDMS oligomers into the interstices can significantly reduce light scattering by reducing the difference in the refractive index between the NW phase and the continuous phase of the NCF. We test this idea by characterizing the transmittance of the ZnO NW arrays before and after LeCaRI via UV-Vis spectroscopy (Fig. 3). A bare glass slide, as well as a PDMS film on glass, are also characterized as references. Fig. 3a clearly shows that infiltration of PDMS oligomers into the ZnO NW arrays significantly enhances the transmission of the NCFs. The enhancement of the transparency upon LeCaRI also can be clearly observed on macroscopic photos of the samples, as shown in Fig. 3b. Remarkably, the transmission of the NCF-24h@150 °C sample shows that this sample is more transmissive than a bare glass slide in most of the visible range, suggesting that the NCF is acting as an anti-reflection coating, as shown in Fig. 3c. We believe such antireflection property is due to the graded transition of refractive index $n_{PDMS} < n_{ZnO}$ across the nanocomposite films, although we do not fully understand the

mechanism behind the suppression of reflection.[27, 47] Digital photograph images of NCFs under light illumination showing

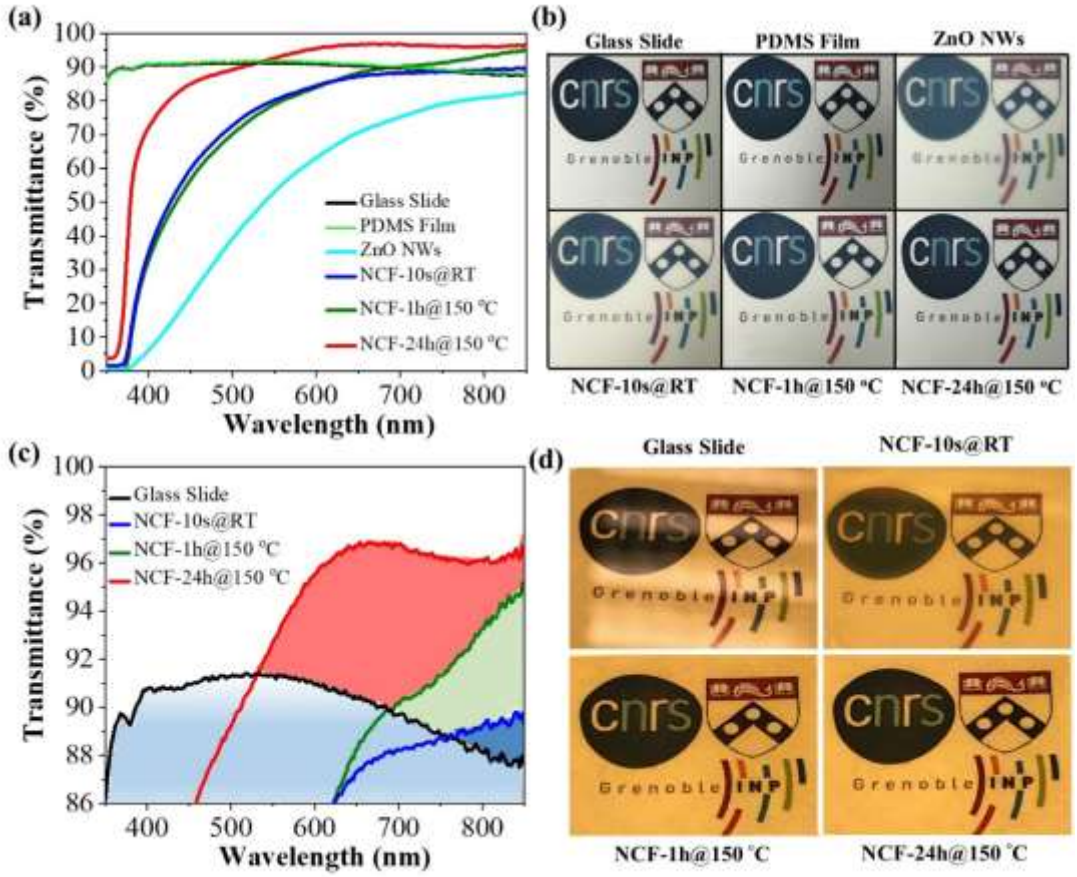

the suppression of reflection compared to glass side clearly demonstrates the anti-reflection property of the NCFs (Fig. 3d).

Fig. 3 (a) Transmittance spectra of glass side, PDMS film, ZnO NWs, and PDMS-infiltrated ZnO NWs, (b) corresponding digital photos of the samples showing their transparency, (c) enlarged transmittance spectra of glass side, NCF-10s@RT, NCF-1h@150 °C, and NCF-24h@150 °C, and (d) digital photograph images of NCFs under light illumination showing the suppression of reflection compared to glass side.

Another useful functionality that can derive from these PDMS/ZnO NW NCFs is their wetting properties. The surface of ZnO NW arrays is highly hydrophilic, whereas the surface of planar PDMS is hydrophobic. Upon infiltration of PDMS via LeCaRI, the surface of the ZnO NW arrays becomes superhydrophobic even after 10 seconds of infiltration at room temperature, as shown in Fig. 4a. Regardless of the infiltration time**,** the surface of the NCFs maintains its superhydrophobicity at least 30 days of storage in the ambient air. When a droplet of water is brought into a dynamic contact with the NCF surface, the droplet does not stick to the surface even if it is pressed onto the surface. In contrast, a water droplet sticks readily to the smooth PDMS film, as shown in Fig. 4b. These results strongly suggest that LeCaRI of PDMS oligomers into the ZnO NW arrays has rendered these surfaces superhydrophobic, likely owing to the combination of surface roughness of the NW array and the hydrophobicity of PDMS, resulting in the so-called Cassie-Baxter state.[48] Even after partial infiltration due to a very short duration (e.g., 10 sec) at room temperature, the surface of NWs is rendered superhydrophobic thanks to the transfer of oligomeric PDMS into the interstices between ZnO NWs. We believe the

presence of even a small amount of PDMS in the interstices facilitates trapping of air and thus renders the surface superhydrophobic. Given the simplicity of the LeCaRI method, superhydrophobic materials can be quickly prepared at room temperature without the use of any extra surface modifiers (e.g., fluorine-containing reagents).

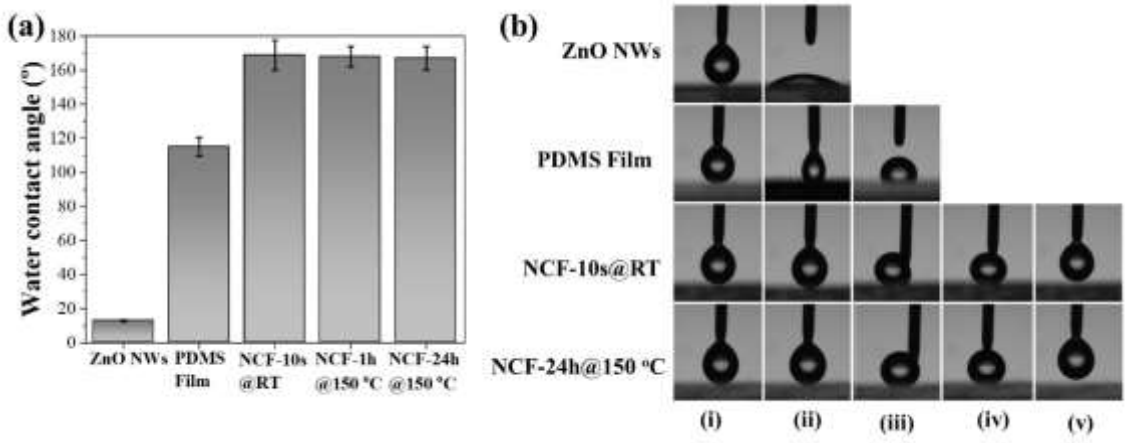

Fig. 4 (a) Static water contact angles on ZnO NWs, PDMS film and ZnO/PDMS LeCaRI NCFs and (b) time-lapse photos showing the wetting properties of the ZnO NWs, PDMS film, and PDMS/ZnO NW NCFs under dynamic contact with a water droplet. A water droplet is brought in contact with samples surface and then pressed on to the surface. Subsequently, the droplet is retracted from the surface. i-v steps represent the initial state (not in contact), initial contact upon approach, pressed contact, right before detachment during retraction, and full retraction, respectively.

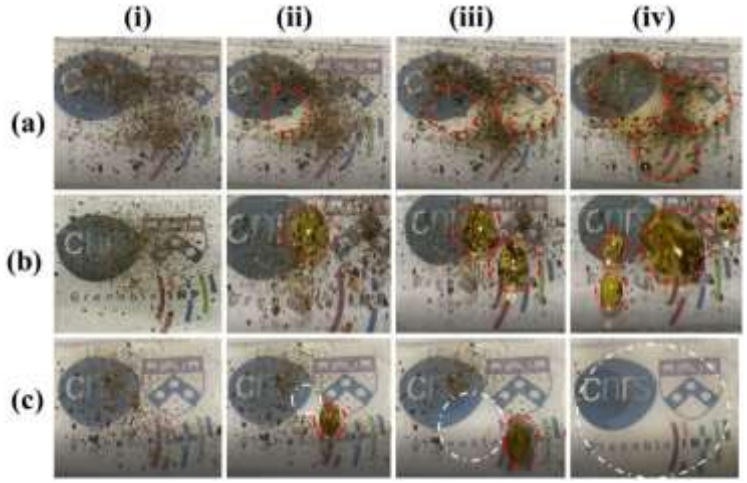

Fig. 5 (i-iv) Sequential photographs showing the removal of soil from the surface of (a) ZnO NWs, (b) PDMS-coated glass, and (c) PDMS/ZnO NW NCF-10s@RT by water droplets with Orange G. Red circles represent shapes and behavior of droplets when they are in contact with the surface of the sample, whereas white circles show the cleaned surface area after exposure to droplets.

A superhydrophobic surface exhibiting a water contact angle (WCA) larger than 150º and easy roll-off of water droplets makes an excellent self-cleaning surface that has a wide range of applications.[49-51] Fig. 5 shows self-cleaning behaviors of ZnO NWs film, PDMS film, and PDMS/ZnO NW NCF-10s@RT when their surfaces are contaminated by soil and

placed horizontally in a plastic container, then subsequently exposed to droplets of Orange G solution (concentration of 5×10^{-5} M, added to facilitate visual inspection of self-cleaning behavior) from a syringe that is placed 5 cm above the sample surface. Droplets readily spread when they are in contact with the highly hydrophilic surface of the ZnO NW arrays (Fig. 5a), whereas droplets stick to the hydrophobic surface of PDMS (Fig. 5b). Owing to its superhydrophobic surface, PDMS/ZnO NW NCF-10s@RT exhibits an excellent self-cleaning behavior by inducing roll-off of water droplets which pick up and remove the contaminants on the surface, as shown in Fig. 5c. Droplets can pick up soil and roll-off from the horizontally placed surface of the PDMS/ZnO NW NCF, which clearly demonstrates its excellent self-cleaning performance.

One of the potential concerns for these NCFs is that PDMS oligomer can be removed when the NCFs are exposed to harsh conditions such as organic solvents. A series of experiments were performed to test the robustness of the PDMS/ZnO NW NCF against various organic solvents by sequentially exposing them to ethanol, acetone, isopropanol, n-hexane, and toluene and water at 37 °C. Fig. 6 clearly shows the exposure to these solvents does not significantly change the wetting properties of the PDMS/ZnO NW NCFs while such treatments induce significant changes in the surface wettability of the reference samples (bare glass slide and ZnO NWs). Upon complete evaporation of the solvents from the surface, the NCF surface still retains its superhydrophobic property. This result shows that the microstructure and composition of the NCFs likely do not experience significant changes even after these NCFs are brought in contact with these common organic solvents. It further indicates that the NCF could be used in later biological applications, by retaining its superhydrophobicity in an aqueous environment at 37 °C for a long time.

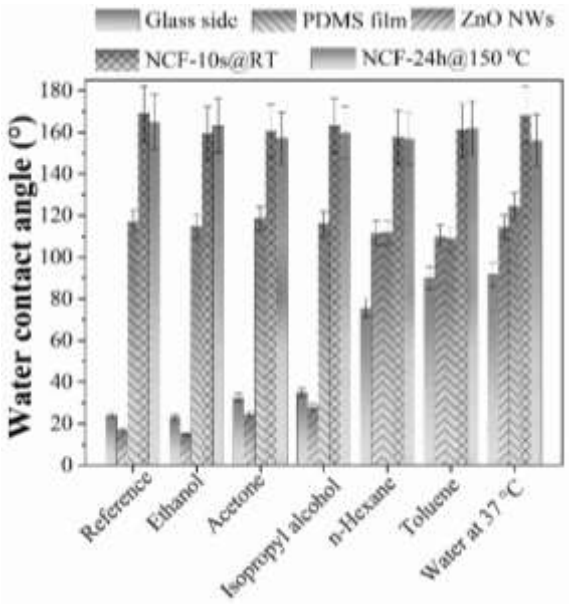

Fig. 6 WCA of samples before and after exposure to a series of organic solvents by sequentially exposing to ethanol, acetone, isopropyl alcohol, n-hexane, and toluene and water at 37 °C.

Another potential concern associated with superhydrophobic materials incorporating photocatalytic materials such as ZnO NWs is the permanent loss of superhydrophobicity upon UV irradiation. We, therefore, test the stability of the superhydrophobic NCF against intense UV irradiation. As shown in Fig. 7a, the NCF-24h@150 °C retains its stable water contact angle of 165° after UV irradiation for several hours. The NCF-10s@RT with infiltrated smaller amount of PDMS shows a slight decrease in its water contact angle value with UV irradiation time; however, the initial superhydrophobic

behavior can be recovered by thermal treatment at 80 °C for 1 h. The results indicate the high stability of the PDMS/ZnO NW NCFs and the easy recovery of superhydrophobicity of the NCF-10s@RT.

One of the most common surface treatment to eliminate and remove contaminants is oxygen plasma. Although this method is very effective in the removal of contaminants, its application on a superhydrophobic surface can potentially lead to permanent loss of the superhydrophobicity. Given the high mobility of PDMS species, we test whether the superhydrophobicity of PDMS/ZnO NW NCF can be recovered after an oxygen plasma treatment. As shown in Fig. 7b, the superhydrophobic of the NCF-10s@RT is lost after oxygen plasma and the surface becomes very hydrophilic with a water contact angle less than 10° likely due to the introduction of polar groups. However, the NCF surface quickly and easily recovers its superhydrophobicity after a simple heat treatment at 80 °C for 30 min. Such recovery of superhydrophobicity can be repeated at least 9 times without reducing the initial superhydrophobicity. According to previous reports on hydrophobicity recovery of PDMS,[11, 52, 53] this phenomenon is due to the diffusion of hydrophobic species to the free surface.

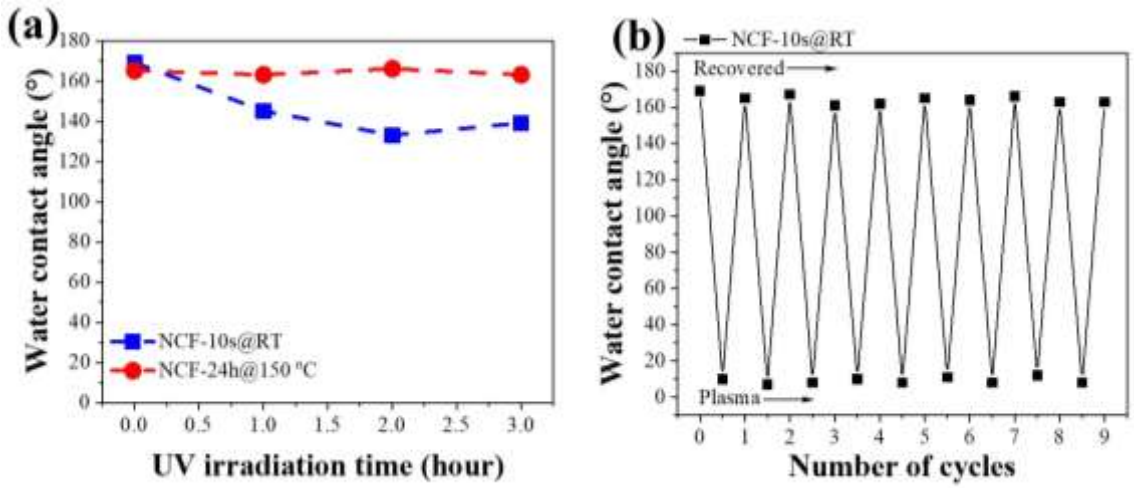

Fig. 7 (a) Effect of UV irradiation on the static water contact angle on PDMS/ZnO NW NCFs. (b) Thermally induced healing of the NCF-10s@RT after repeated oxygen plasma treatment of NCF-10s@RT.

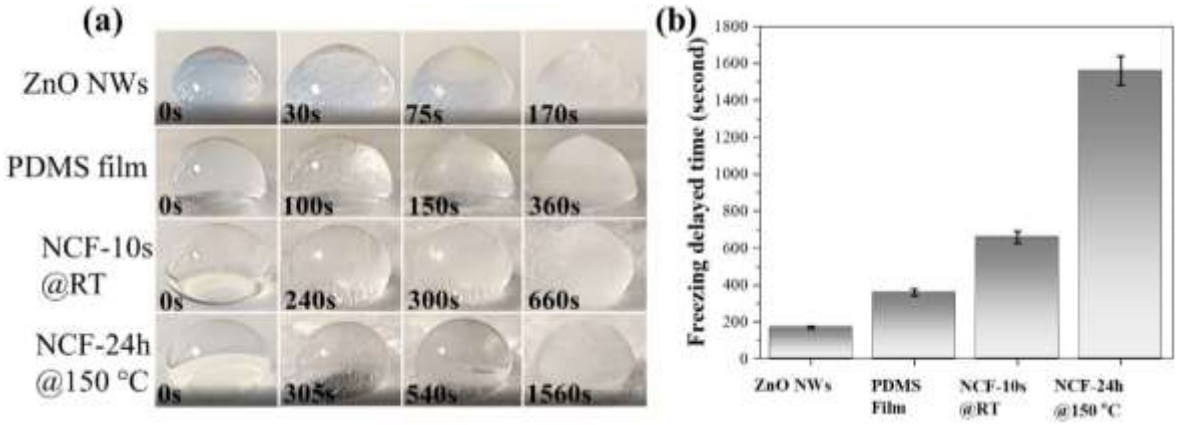

Fig. 8 (a) Ice accumulation on the surface of ZnO NWs, PDMS film, NCF-10s@RT and NCF-24h@150 °C at −15 ± 1 °C environment with the delayed freezing time recorded by observing the non-transparency of the water droplets (b) Freezing time of ZnO NWs, PDMS film on glass, NCF-10s@RT, and NCF-24h@150 °C at -15 °C.

Ice accumulation on the solid surface can pose serious problems in many industrial applications. For example, ice formation on aircraft and electric transmission lines could cause major complications. Moreover, accreted ice on surfaces can significantly decrease heat transfer efficiency in refrigerators/heat exchangers.[54-56] It is, thus, highly desirable to impart an anti-icing property to various solid surfaces. To show the potential of our nanocomposite films toward anti-icing applications, we perform an anti-icing experiment to determine the time it takes for a water droplet to freeze on different surfaces. The freezing delay time is defined as the time between physical contact of a water droplet with a subcooled substrate and the onset of freezing.[54] The samples are placed on a thermally controlled stage, and they are cooled down to −15 °C. After 10 min to ensure thermal equilibrium, water droplets are placed on the sample surface, and the freezing times of water droplets on different samples are recorded. Initially, the droplets are clear and transparent on the surface of the samples. However, with time, white ice crystals appear in the droplet which eventually turns into an opaque ice crystal. Fig. 8a shows that the PDMS/ZnO NWs NCFs exhibit a superior anti-icing property compared to ZnO NWs and PDMS film, significantly delaying the formation of ice nuclei and reducing the growth rate of ice crystals. As shown in Fig. 8b, the freezing times of PDMS/ZnO NWs NCFs are much longer than those of the ZnO NWs and PDMS film. The results clearly demonstrate the excellent ability of ZnO/PDMS NCFs to suppress ice formation and accumulation.

This significant increase in the freezing time of NCFs compares to that of ZnO NWs and PDMS film, is likely due to the superhydrophobicity, reducing the contact area between the water droplet and the surface, and therefore dramatically reducing heat transfer between the NCFs @ -15°C and the droplet that is surrounded by air @ 20°C.[57, 58] In addition, the remarkable delayed-icing ability of the NCF-24h@150 °C compared to that of the NCF-10s@RT, we believe, is due to the different amounts of PDMS oligomers infiltrated into nanowires via the LeCaRI process. The infiltrated PDMS layer at the top surface of the NCF-10s@RT is thinner compared to that of the NCF-24h@150 °C, as clearly shown in the SEM images and especially in the EDS mapping image (Fig. 2c, f, and i). Considering the thermal transport path in the ZnO NW arrays, heat transfer occurs through the vertically aligned ZnO NWs from the copper substrate to the water droplet at the surface. Thus, the thicker the infiltrated PDMS layer at the top surface is, the bigger the heat transfer resistance will be to the water droplet, resulting in enhanced delayed-icing.We believe this is the main reason for the efficient delay-icing ability of the NCF-24h@150 °C with complete infiltration compared to that of the NCF-10s@RT with partial infiltration. Significantly longer freezing times indicate that ZnO/PDMS NCFs could be highly advantageous in applications that require de-icing since water droplets can easily roll off with slight tilt angles or with mild vibration before they undergo freezing.

CONCLUSIONS AND OUTLOOK

In conclusion, we report a new method to fabricate nanocomposite films retaining the vertical alignment of ZnO NWs via leaching-enabled capillary rise infiltration (LeCaRI). PDMS-infiltrated vertically aligned ZnO NWs NCFs exhibit high transparency, anti-reflection, superhydrophobic, self-cleaning, and anti-icing properties and also can retain their superhydrophobicity even after being exposed to organic solvents, or intense-UV irradiation and oxygen plasma treatment. Because the growth of ZnO NWs can be performed via solution-based methods and LeCaRI is a process that requires simple contact of PDMS with the ZnO NW array, we believe this process could potentially be scaled up to enable continuous

fabrication of these versatile NCFs. Moreover, the process can be used to produce NCFs with horizontally or randomly oriented NWs.

EXPERIMENTAL

Materials

High aspect ratio ZnO NW arrays are hydrothermally grown onto a seed layer deposited on a glass substrate using a sol-gel process as previously reported in our works.[43-45] The ZnO NW arrays possess a diameter, a length, and a vertical angle of 73±16 nm, 1.2±0.17 μm, and 89±12° respectively, on glass slides (2.5 cm × 2.5 cm) (see the SI for the detailed description of preparation and statistical analysis of the geometry of ZnO NWs). Poly(dimethylsiloxane) (PDMS), Sylgard 184, was purchased from Sigma-Aldrich in the form of a Silicone Elastomer Kit composed of a base and a curing agent to be mixed in a 10 (base): 1 (curing agent) ratio by weight. Then they are diluted in Hexane with a 1:1 ratio for ease of handling. The diluted PDMS was poured into Petri dish, then baked at 80 °C for 2 h for curing of PDMS. By using a steel tweezer, the PDMS elastomer can be peeled off and used for infiltration experiments.

Fabrication of Polymer/ZnO NW array NCFs via LeCaRI

Before LeCaRI, ZnO NW arrays on glass slides are placed in the oven at 540 °C for 5 min to remove organic contaminants and water vapor, which exists between adjacent nanowires. ZnO NW arrays are brought in contact with a slab of PDMS elastomer (2.5 cm × 2.5 cm × 0.25 cm) to induce the transfer of uncross-linked and mobile chains from the elastomer network into the interstices of the ZnO NW arrays. To maximize the number of transferred oligomers, the sample with PDMS elastomer atop ZnO NW arrays is placed in the oven maintained at 150 °C. Subsequently, the oligomer infiltrated ZnO NW arrays are heated at a maintained temperature of 80 °C for 1 h to cure the unreacted chains transferred into the interstices of ZnO NW arrays.

Characterization

Scanning electron microscopy (SEM) images were taken on a FEI QUANTA 250 to characterize the morphology of ZnO NW arrays before and after LeCaRI. SEM images are captured at an accelerating voltage of 5 kV and a working distance of 10 mm. Energy dispersive spectroscopy (EDS) is used to acquire the EDS composition spectra. Raman scattering spectra are obtained using a Jobin Yvon/Horiba Labram spectrophotometer equipped with a liquid nitrogen cooled CCD detector. A He–Ne laser is used to induce a 632.8 nm excitation line. The excitation laser is focused on an area smaller than 1 μm^2 using a 50 × long working distance objective. Raman scattering spectra are calibrated using a silicon reference sample with a theoretical value of 520.7 cm^{-1} at room temperature. Optical transmittance is measured in the wavelength range of 350 to 900 nm using a Perkin Elmer UV-Vis-Near IR Lambda 950 spectrophotometer. The static water contact angle (CA) values were measured using a Krüss, DSA10-MK2 goniometer connected to a video camera. Five water droplets of 5 μL volume were dropped on different points of the sample surface using a microsyringe, and water contact angle values were measured. The CA values were calculated and collected by using the drop shape analysis software (DSA4). The plasma treatment experiments are conducted using oxygen plasma instrument (Evactron Decontaminator RF Plasma cleaner, XEI Scientific) at a power of 12 W for 5 min.

Solvent resistance study

A series of experiment has been implemented to test the anti-fouling to relatively low boiling point organic solvents in sequence with ethanol, acetone, and toluene and water at 37 °C. Samples were immersed in a solvent container for 10 min, then placed in air for 2 min for evaporation of the solvents. For the case of water, the samples underwent solvents

exposure were immersed in a water bath in a humidity chamber kept at 37 °C and 40 % relative humidity for 60 h. After each experiment, the wettability of the samples was evaluated according to the procedure described in the water contact angle measurement.

Self-cleaning

To see the self-cleaning performance of samples, the sample surface was contaminated by soils collected outside our building. After soils contamination of the surface, samples are placed horizontally in a plastic container, then subsequently exposed to droplets of Orange G solution (concentration of 5×10^{-5} M) from a syringe at the height of 5 cm from the sample surface to the syringe needle.

UV irradiation

During this test the samples were illuminated by three UV lamps (Philips, λ = 360, 310, and 250 nm, respectively). The samples were placed 1 cm under the UV lamps for 3 h. The process is conducted in a humidity chamber at 20 °C and 40 % relative humidity. The water CA values are measured at regular intervals (30 min) of exposure.

Anti-icing test

The samples were placed on a thermally controlled copper stage set horizontally in a controlled humidity and temperature chamber, then freezing the stage containing the samples to a temperature at −15 °C. After 10 min to ensure the sample surface reach the supercool temperature, water droplets were placed on the sample surface to test the anti-icing property by observing the change of water droplets from transparent to opaque.

CONFLICTS OF INTEREST

There are no conflicts to declare.

ACKNOWLEDGEMENTS

The authors acknowledge the support of the Chair of excellence from the “UGA Fondation Nanosciences”. This work was also supported by NSF PIRE grant 1545884. H.H. Tran would like to thank Dr. O. Chaix and Dr. V.H. Nguyen for Raman measurements and technical discussions, respectively.

REFERENCES

1. Y. R. Huang, Y. Jiang, J. L. Hor, R. Gupta, L. Zhang, K. J. Stebe, G. Feng, K. T. Turner and D. Lee, *Nanoscale*, 2015, **7**, 798-805.
2. N. Manohar, K. J. Stebe and D. Lee, *ACS Macro. Lett.*, 2017, **6**, 1104-1108.
3. J. L. Hor, Y. Jiang, D. J. Ring, R. A. Riggleman, K. T. Turner and D. Lee, *ACS Nano*, 2017, **11**, 3229-3236.
4. H. Wang, J. L. Hor, Y. Zhang, T. Liu, D. Lee and Z. Fakhraai, *ACS Nano*, 2018, 12, 5580-5587.
5. J. L. Hor, H. Wang, Z. Fakhraai and D. Lee, *Soft. Matter.*, 2018, **14**, 2438-2446.
6. R. B. Venkatesh, S. H. Han and D. Lee, *Nanoscale Horiz.*, 2019, 4, 933-939.
7. Y. Jiang, J. L. Hor, D. Lee and K. T. Turner, *ACS Appl. Mater. Interfaces*, 2018, **10**, 44011-44017.
8. Y. Qiang, N. Manohar, K. J. Stebe and D. Lee, *Mol. Syst. Des. Eng.*, 2018, **3**, 96-102.
9. R. Hoffmann, V. Baric, H. Naatz, S. O. Schopf, L. Mädler and A. Hartwig, *ACS Appl. Nano Mater.,* 2019, 2, 2273-2282.
10. W. Chen, L. Qu, D. Chang, L. Dai, S. Ganguli and A. Roy, *Chem. Commun.*, 2008, 2, 163-165.
11. S. Peng, W. Meng, J. Guo, B. Wang, Z. Wang, N. Xu, X. Li, J. Wang and J. Xu, *Langmuir*, 2019, **35**, 2760-2771.
12. E. P. Chan, W. D. Mulhearn, Y. R. Huang, J. H. Lee, D. Lee and C. M. Stafford, *Langmuir*, 2014, **30**, 611-616.

13. B. Yeom, T. Sain, N. Lacevic, D. Bukharina, S. H. Cha, A. M. Waas, E. M. Arruda and N. A. Kotov, *Nature*, 2017, **543**, 95-98.
14. M. T. Barako, S. G. Isaacson, F. Lian, E. Pop, R. H. Dauskardt, K. E. Goodson and J. Tice, *ACS Appl. Mater. Interfaces,* 2017, **9**, 42067-42074.
15. D. Fragouli, R. Buonsanti, G. Bertoni, C. Sangregorio, C. Innocenti, A. Falqui, D. Gatteschi, P. D. Cozzoli, A. Athanassiou and R. Cingolani, *ACS Nano*, 2010, **4**, 1873-1878.
16. X. Qu, H. Feng, S. Liu, Y. Yang and C. Ma, *Inorg. Chem. Commun.*, 2018, **98**, 174-179.
17. M. K. Kim, D. K. Yi and U. Paik, *Langmuir*, 2010, **26**, 7552-7554.
18. X. Meng, L.-T. Zhou, J.-X. Zhu, J. Song, X.-R. Wang and Z.-P. Qiao, *Appl. Phys. Lett.*, 2008, **93**, 263101.
19. K. E. Plass, M. A. Filler, J. M. Spurgeon, B. M. Kayes, S. Maldonado, B. S. Brunschwig, H. A. Atwater and N. S. Lewis, *Adv. Mater.*, 2009, **21**, 325-328.
20. J. Yuan, X. Liu, O. Akbulut, J. Hu, S. L. Suib, J. Kong and F. Stellacci, *Nat. Nanotechnol.*, 2008, **3**, 332-336.
21. Y. Yao, X. Zhu, X. Zeng, R. Sun, J. B. Xu and C. P. Wong, *ACS Appl. Mater. Interfaces*, 2018, **10**, 9669-9678.
22. X. Jing and Z. Guo, *Nanoscale*, 2019, **11**, 8870-8881.
23. C. M. Taylor, A. Ramirez-Canon, J. Wenk and D. Mattia, *J. Hazard. Mater.*, 2019, **378**, 120799.
24. L. Zhang, Y. Wang, H. Wu, M. Hou, J. Wang, L. Zhang, C. Liao, S. Liu and Y. Wang, *Nanoscale*, 2019, **11**, 8319-8326.
25. B. Wen, J. E. Sader and J. J. Boland, *Phys. Rev. Lett.*, 2008, **101**, 175502.
26. Q. Wan, Q. H. Li, Y. J. Chen, T. H. Wang, X. L. He, J. P. Li and C. L. Lin, *Appl. Phys. Lett.,* 2004, **84**, 3654-3656.
27. Y. Gao, I. Gereige, A. El Labban, D. Cha, T. T. Isimjan and P. M. Beaujuge, *ACS Appl. Mater. Interfaces,* 2014, **6**, 2219-2223.
28. S. Ma, R. Li, C. Lv, W. Xu and X. Gou, *J. Hazard. Mater.*, 2011, **192**, 730-740.
29. T.-J. Kuo, C.-N. Lin, C.-L. Kuo and M. H. Huang, *Chem. Mater.*, 2007, **19**, 5143-5147.
30. F. H. Chu, C. W. Huang, C. L. Hsin, C. W. Wang, S. Y. Yu, P. H. Yeh and W. W. Wu, *Nanoscale*, 2012, **4**, 1471-1475.
31. S. Chu, D. Li, P. C. Chang and J. G. Lu, *Nanoscale Res. Lett.*, 2011, **6**, 38.
32. F. L. Boughey, T. Davies, A. Datta, R. A. Whiter, S. L. Sahonta and S. Kar-Narayan, *Nanotechnology*, 2016, **27**, 28LT02.
33. S. Shekhar, P. Stokes and S. I. Khondaker, *ACS Nano*, 2011, **5**, 1739-1746.
34. L. Li, H. Fan, C. Hou, Q. Zhang, Y. Li, H. Yu and H. Wang, *ACS Appl. Nano Mater.*, 2019, **2**, 1466-1471.
35. M. Gong, J. Zhang and S. Ren, *Nanotechnology*, 2018, **29**, 345602.
36. Z. Liu, Z. Weng, Z. F. Zhai, N. Huang, Z. J. Zhang, J. Tan, C. Jiang, D. Jiao, G. Tan, J. Zhang, X. Jiang, Z. Zhang and R. O. Ritchie, *Acta. Biomater.*, 2018, **81**, 267-277.
37. A. Hourlier-Fargette, J. Dervaux, A. Antkowiak and S. Neukirch, *Langmuir*, 2018, **34**, 12244-12250.
38. L. Yang, N. Shirahata, G. Saini, F. Zhang, L. Pei, M. C. Asplund, D. G. Kurth, K. Ariga, K. Sautter, T. Nakanishi, V. Smentkowski and M. R. Linford, *Langmuir*, 2009, **25**, 5674-5683.
39. A. L. Briseno, M. Roberts, M. M. Ling, H. Moon, E. J. Nemanick and Z. Bao, *J. Am. Chem. Soc.*, 2006, **128**, 3880-3881.
40. K. J. Regehr, M. Domenech, J. T. Koepsel, K. C. Carver, S. J. Ellison-Zelski, W. L. Murphy, L. A. Schuler, E. T. Alarid and D. J. Beebe, *Lab. Chip.*, 2009, **9**, 2132-2139.
41. J. H. Kim, H. S. Hwang, S. W. Hahm and D. Y. Khang, *Langmuir*, 2010, **26**, 13015-13019.
42. A. Carlson, A. M. Bowen, Y. Huang, R. G. Nuzzo and J. A. Rogers, *Adv. Mater.*, 2012, **24**, 5284-5318.
43. T. Demes, C. Ternon, F. Morisot, D. Riassetto, M. Legallais, H. Roussel and M. Langlet, *Appl. Surf. Sci.*, 2017, **410**, 423-431.
44. T. Demes, C. Ternon, D. Riassetto, V. Stambouli and M. Langlet, *J. Mater. Sci.*, 2016, **51**, 10652-10661.
45. T. Demes, C. Ternon, D. Riassetto, H. Roussel, L. Rapenne, I. Gélard, C. Jimenez, V. Stambouli and M. Langlet, *J. Phys. Chem. Solids*, 2016, **95**, 43-55.
46. H. Yoshikawa and S. Adachi, *Jpn. J. Appl. Phys.*, 1997, **36**, 6237-6243.
47. D. H. Raguin and G. M. Morris, *Appl. Opt.*, 1993, **32**, 1154-1167.
48. A. B. D. Cassie and S. Baxter, *Trans. Faraday Soc.,* 1944, **40**, 546.
49. X. M. Li, D. Reinhoudt and M. Crego-Calama, *Chem. Soc. Rev.*, 2007, **36**, 1350-1368.
50. L. Wen, Y. Tian and L. Jiang, *Angew. Chem. Int. Ed. Engl.,* 2015, **54**, 3387-3399.
51. R. Blossey, *Nat. Mater.*, 2003, **2**, 301-306.
52. D. Bodas and C. Khan-Malek, *Sens. Actuator B-Chem.,* 2007, **123**, 368-373.
53. D. T. Eddington, J. P. Puccinelli and D. J. Beebe, *Sens. Actuator B-Chem.,* 2006, **114**, 170-172.
54. Q. Li and Z. Guo, *J. Mater. Chem. A*, 2018, **6**, 13549-13581.
55. L. Mishchenko, B. Hatton, V. Bahadur, J. A. Taylor, T. Krupenkin and J. Aizenberg, *ACS Nano*, 2010, **4**, 7699-7707.
56. J. Lv, Y. Song, L. Jiang and J. Wang, *ACS Nano*, 2014, **8**, 3152-3169.
57. V. J. Rico, C. Lopez-Santos, M. Villagra, J. P. Espinos, G. F. de la Fuente, L. A. Angurel, A. Borras and A. R. Gonzalez-Elipe, *Langmuir*, 2019, **35**, 6483-6491.
58. L. Wang, C. Teng, J. Liu, M. Wang, G. Liu, J. Y. Kim, Q. Mei, J. K. Lee and J. Wang, *J. Ind. Eng. Chem.*, 2018, **62**, 46-51.

Scalable fabrication of multifunctional nanocomposite films with vertically aligned ZnO nanowires via inducing leaching-enabled capillary rise infiltration (LeCaRI).